INVESTIGATION OF HIGH Q L-MODE PLASMA OPERATION SUSTAINED BY ENHANCED PELLET FUELLING IN ITER

J. Zhang, G. Zhuang

University of Science and Technology of China

Hefei, China

Email: jiez111@ustc.edu.cn

F. Koechl, A. Polevoi

ITER Organization

Abstract

In this work, we attempt to increase core density by enhanced pellet fueling to investigate the possibility of high Q L-mode plasma operation for ITER. JINTRAC integrated modeling suite is adopted as the modeling tool, with the HPI2 module for pellet fueling modeling. We compare results obtained with the Bohm-gyro-Bohm (BgB) scaling-based model against the TGLF-SAT2 model, the interpretive impurity model against the predictive SANCO impurity transport model, and the continuous pellet model against the discrete pellet model based on the HPI2 code. The confinement in ITER high density L-mode predicted by the TGLF-SAT2 model is in general much better than that with the BgB scaling, resulting in a significantly larger Q. Fusion performances such as Pfus and Q change only slightly when changing from the interpretive impurity model to the predictive SANCO model, or changing from the continuous pellet model to the discrete HPI2 pellet model. The highest Q obtained for these ITER high density L-mode simulations is ~5, which is quite amazing and reveals the potentials of high Q L-mode operation for ITER and demo reactors.

1. INTRODUCTION

When designing fusion reactors, L-mode operation is usually discarded, because fusion power performance in L mode plasma is predicted to be low according to L-mode confinement scaling. However, L-mode reactor conditions might still be worth being examined by means of integrated modelling, trying to explore means for optimization in terms of achievable fusion gain Q by changing some actuators, such as auxiliary heating and particle fueling methods. In addition, high Q L-mode operation is worth being explored as back-up option if ELM-suppressed or ELM-mitigated H-mode operation turns out to be challenging. Our methods for optimization in terms of achievable fusion gain Q in L mode include enhancing pellet fueling to increase density, increasing auxiliary heating power, and optimizing impurity content.

2. SIMULATION SETUP

Simulations in this work are performed with High-Fidelity Plasma Simulator (HFPS), which is an IMASified JETTO [1] version. The simulation set-ups are summarized in Table 1.

Table 1. Summary of simulation setups and the modules implemented in the integrated modeling.

- 1 -

IAEA-TH-P/3025

Description	Simulation tool / setup
Integrated Modeling Suite	High-Fidelity Plasma Simulator (HFPS) (an IMASified
	JETTO version)
Plasma Boundary Shape	Full-bore ITER
Equilibrium	ESCO
Turbulent Transport in Core	TGLF - SAT2
Neoclassical Transport	NCLASS
Transport Equations Variables	j, T_e, T_i, n_D and n_T
Toroidal Momentum	Interpretive
EC Heating and ECCD	Prescribed central Gaussian for EC heating
	GRAY-based scaling for ECCD
NB Heating	PENCIL
IC Heating	PION
Core Volume-averaged Electron Density	Feedback controlled by pellets (continuous model with
Control	Gaussian particle source or discrete pellet model with
	HPI2 code)
Neutral Influx at Plasma	Assumed to be negligible
Boundary Conditions	n_e and n_i at plasma boundary with ITER-SOLPS scaling
	[2]
Impurities Treatment	Interpretive or self – consistently predicted with
	SANCO module
Radiation Profile	Prescribed flat and scaled to fixed radiation fraction
Fusion Reactions and Alpha	SIMOD
Thermalization	

3. RESULTS AND ANALYSES

3.1 Simulation scans with BgB scaling

3.1.1 Scan of Paux and target ne

Firstly, the empirical Bohm gyro-Bohm scaling is adopted for modeling energy and particle transport process.

The auxiliary heating power, P_{aux} , and the target density described by the Greenwald density fraction, n_e/n_{GW} , are scanned respectively with a fixed radiation fraction, $P_{rad}/P_{inp} = 0.3$, where P_{rad} is the total radiation power and P_{inp} is the total auxiliary heating power. Table 2 lists inputs of the auxiliary heating power and the target Greenwald density fraction as well as the corresponding outputs of fusion power, P_{fus} , and fusion gain, Q_{fus} , in different simulation cases. Obviously, high density is favorable for high fusion performance since $P_{fus} \propto n^2$. It should be noted that the net loss power, P_{net} , may exceed the L-H transition power threshold, P_{LH} , with increasing auxiliary heating power. However, the plasma is enforced to be at L mode in all simulations.

Table 2. Inputs of the auxiliary heating power in unit MW, and the target Greenwald density fraction as well as the corresponding outputs such as P_{fus} and Q_{fus} in different simulation cases.

Case	P_{EC}	P_{NB}	P _{IC}	P _{rad} /P _{inp}	$f_{\mathit{GW}}, \%$	P_{LH}	P_{net} $/P_{LH}$	max (P_{fus})	Q_{fus}
run50	60	0	0	0.3	40	42	1.1	8	0.13
run50					60	54	0.92	28	0.47

Case	P _{EC}	P_{NB}	P _{IC}	P _{rad} /P _{inp}	$f_{\mathit{GW}}, \%$	P_{LH}	P_{net} $/P_{LH}$	$max (P_{fus})$	Q_{fus}
run50					90	78	0.74	75	1.25
run51a	27	33	0	0.3	60	54	0.99	40	0.67
run51a					90	78	0.72	50	0.83
run52a	60	33	0	0.3	60	54	1.5	52	0.56
run52a					90	78	1.1	112	1.20
run53a corr	60	33	20	0.3	60	54	1.78	70	0.62
run53a corr					90	78	1.34	160	1.42
run53b corr	60	33	20	0.1	60	54	2.28	80	0.71
run53b corr					90	78	1.78	190	1.68

3.1.2 Scan of radiation fraction and target density with $P_{aux} = 113 \text{ MW}$

The radiation fraction and the target density are then scanned respectively, with a high auxiliary heating power of $P_{aux} = 113$ MW, where $P_{EC} = 60$ MW, $P_{NB} = 33$ MW, and $P_{IC} = 20$ MW are applied. Table 3 lists the inputs of the radiation fraction and the target Greenwald density fraction $f_{GW} = n_e/n_{GW}$, the pellet fueling rate to maintain the target density, the power throughput crossing the separatrix P_{sep} , the energy confinement factor H98(y, 2), the L-H transition power P_{LH} , the ratio P_{sep} / P_{LH} , as well as the corresponding outputs of P_{fus} and Q_{fus} in different simulation cases.

When $f_{GW} = 60\%$ or 90%, the confinement improves with increasing radiation fraction as expected, but P_{fus} and Q_{fus} decrease instead due to stronger radiation and more dilution with increasing impurities. At very high density with $f_{GW} = 180\%$, the confinement does not improve with higher Z_{eff} , and P_{fus} and Q_{fus} decrease significantly due to much stronger radiation and more dilution with increasing impurities. These scans have indicated that the detrimental effect of radiation and dilution on fusion performances might outweigh the confinement improvement which might also be limited by the requirement of a very high radiation fraction with high Z_{eff} .

Table 3. Inputs and outputs in different simulation cases.

Case	P _{rad} /P _{inp}	$f_{\mathit{GW}}, \%$	S_{pel}	P_{sep}	$H_{98}(y,2)$	P_{LH}	P _{sep} /P _{LH}	max (P_{fus})	Q_{fus}
run54	0.1	60	3.50e22	125	0.45	54	2.31	80	0.71
		120	8.00e22	145	0.47	92	1.58	230	2.04
		180	1.40e23	180	0.55	124	1.45	400	3.54
run54a	0.3	60	3.50e22	98	0.48	54	1.81	80	0.71
		120	8.00e22	110	0.5	92	1.20	195	1.73
		180	1.30e23	125	0.54	124	1.00	290	2.57
run54b	0.5	60	3.50e22	72	0.53	54	1.33	78	0.69
		120	7.70e22	78	0.53	92	0.85	160	1.42
		180	1.24e23	81	0.53	124	0.65	192	1.70
run54c	0.7	60	3.50e22	45	0.55	54	0.83	75	0.66
		120	7.50e22	48	0.56	92	0.52	122	1.08
		180	1.14e23	49	0.55	124	0.40	132	1.17

3.2 Results with BgB scaling-based v.s. TGLF-SAT2 model

In this section, BgB scaling-based transport model is replaced with the TGLF-SAT2 transport model to predict transport process self-consistently with other settings kept the same with simulation cases in section 3.1. Figure 1 shows time traces of the energy confinement factor H98(y, 2), the fusion gain, the electron temperature, and the total pellet source rate controlling the volume averaged electron density through a feedback manner, predicted by the BgB scaling-based (blue) and the TGLF-SAT2 model (green) respectively for the simulation case run53acorr listed in Table 3, with $P_{aux} = 113$ MW and $f_{GW} = 90\%$. The most significant difference between simulation results with two models is the confinement level, which leads to a large jump and oscillation in parameters when changing the transport model to TGLF-SAT2. The predicted H98(y,2) is ~0.65 with TGLF-SAT2 model, much higher than that predicted with BgB scaling (H ~ 0.5). $H \le 0.5$ is the typical expectation for L-mode. With much better confinement, Qfus increases from 1.2 to ~1.7, by about 40%. And Q_{fus} may be further increased with higher n_{sep} , which depends on such parameters as power to SOL, impurity fraction, gas puffing and pumping [2].

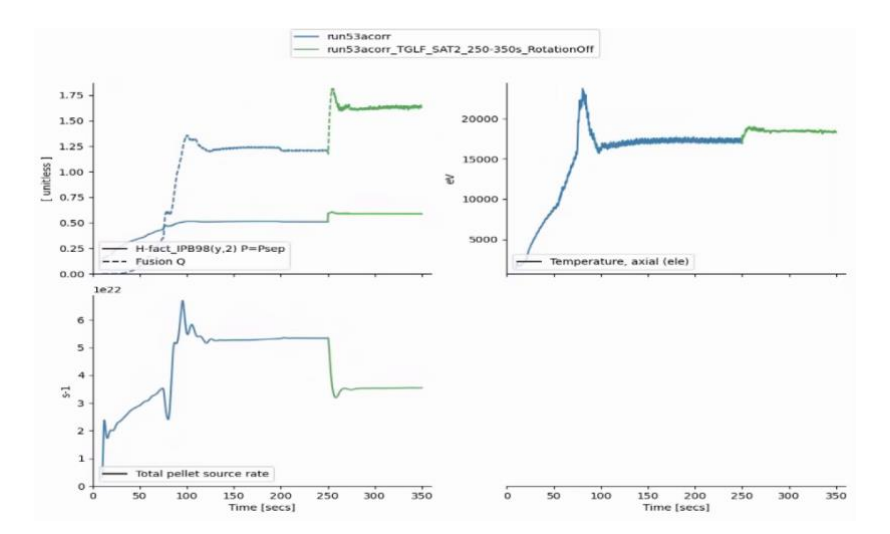


FIG. 1. Time traces of the energy confinement factor H98(y, 2), the fusion gain, the electron temperature, and the total pellet source rate controlling the volume averaged electron density through a feedback manner, predicted by the BgB scaling (blue) and the TGLF-SAT2 model (green) respectively for the simulation case run53acorr listed in Table 3 with $P_{\text{aux}} = 113$ MW and $f_{\text{GW}} = 90\%$.

The highest energy gain factor is $Q_{fus} = 3.54$ predicted with BgB scaling for the case run54 among all simulation cases listed in Table 2 and Table 3. When the transport model is changed to TGLF-SAT2 in this case, the predicted confinement factor can reach a high value as H98(y,2) ~0.75, much higher than that predicted with BgB scaling-based model H98(y,2) ~0.55, as shown in figure 2. With much better confinement, Q_{fus} increases from 3.54 to ~5.0. In this case, $P_{aux} = 113$ MW, $f_{GW} = 150\%$, and $P_{rad}/P_{inp} = 0.1$. Z_{eff} is scanned to explore its influence on confinement and fusion performances.

J. Zhang et al., Preprint

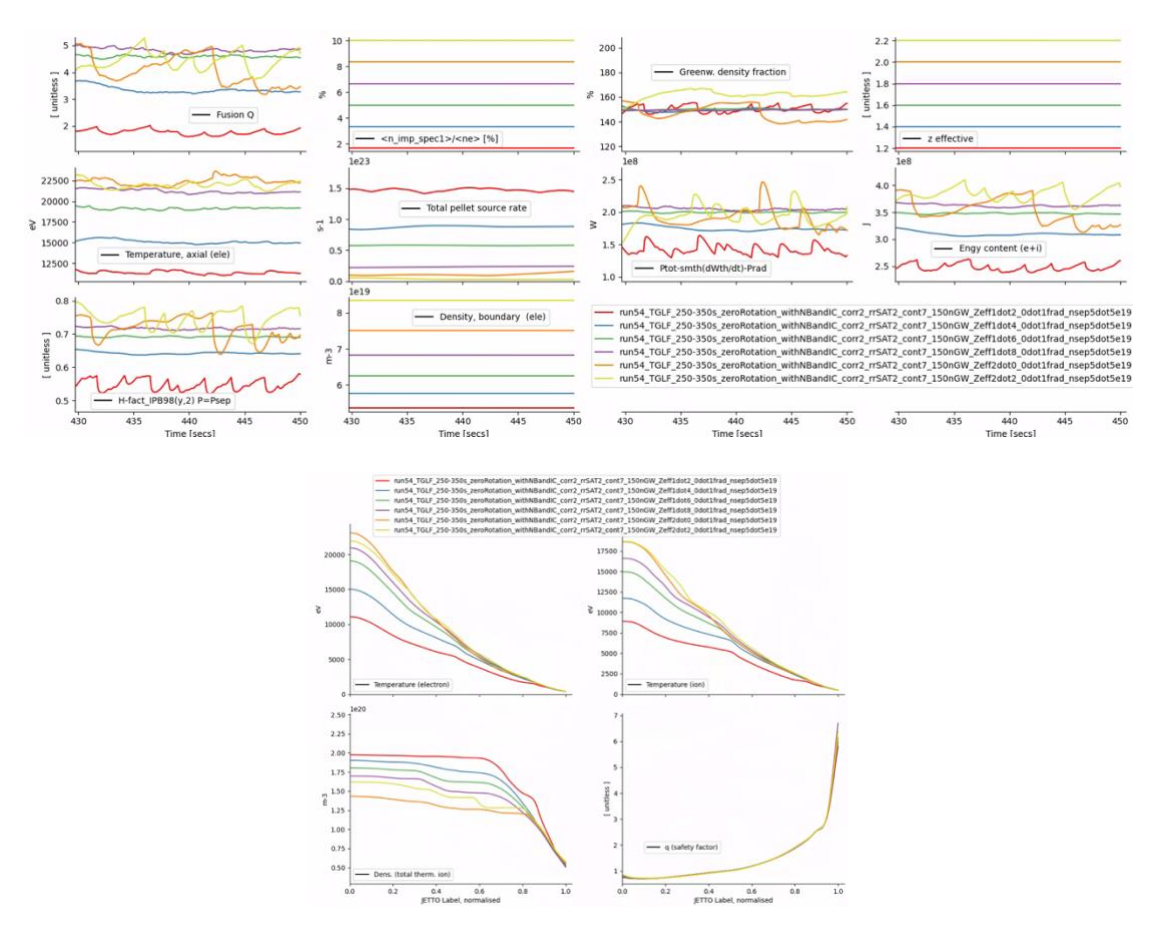


FIG. 2. Time traces of the fusion gain $Q_{\rm fus}$, the impurity concentration, the Greenwald density fraction, Z_{eff} , the axial electron temperature, the total pellet source rate, $P_{tot} - smth\left(\frac{dw_{th}}{dt}\right) - P_{rad}$, the energy content, the energy confinement factor H98(y, 2), and the boundary electron density predicted by JETTO with the TGLF-SAT2 model for the simulation case run54 listed in Table 3 with $Z_{eff} = 1.2$ (red), 1.4 (blue), 1.6 (green), 1.8 (purple), 2.0 (orange) and 2.2 (yellow) respectively, with $P_{\rm aux} = 113$ MW, $f_{\rm GW} = 150\%$ and $P_{\rm rad}/P_{\rm inp} = 0.1$. Comparisons of profiles of the electron temperature, ion temperature, total thermal ion density and safety factor at the end of the simulation are also shown.

Influences of Z_{eff} on H98(y,2) and Q_{fus} are clearly shown in figure 2. In the range of Z_{eff} scanned, confinement improves with increasing Z_{eff} . H98(y,2) increases from 0.55 to ~0.75 when Z_{eff} increases from 1.2 to 2.2, and saturates at this value. Q_{fus} first increases and then decreases when Z_{eff} increases from 1.2 to 2.2, reaching a highest value of ~5, which is quite amazing for L-mode scenario. The trend in Q_{fus} is due to the competition between confinement improvement, radiation increase and main ion density dilution with increasing Z_{eff} . With increasing Z_{eff} , the averaged ion density decreases due to dilution effect, however, the axial ion density first decreases and then increases. The increased axial ion density may be explained by confinement improvement and stronger inward transport of main ions. With increasing Z_{eff} , the ion temperature, especially the axial ion temperature, increases due to confinement improvement, which is also beneficial to fusion performances.

3.3 Results with impurities treated by SANCO

In this section, the interpretive impurity transport model is replaced with the SANCO model to predict impurity transport process self-consistently, and TGLF-SAT2 transport model is adopted to predict transport process of main particles self-consistently, with other settings kept the same with simulation cases in section 3.1. Three species of impurities are included in simulations, i.e., He, Be and W. There is helium source due to fusion reaction in the core, and an escape velocity is assumed as the outside boundary condition for He. Zero escape velocity is assumed as the outside boundary condition for Be and W. It is also assumed that there are no sources from the edge. Thus, the impurity density can evolve to a steady state. The ionization states of W are bundled as six super stages to speed up the simulation. The atomic and radiation data of the super states come from the superstate file from ADAS.

Results obtained with the SANCO module are shown in figure 3. This case has the highest Q_{fus} obtained so far for stationary conditions with TGLF-SAT2-EM applied at $\rho_{norm} < 0.7$ and TGLF-SAT2 without consideration of electro-magnetic perturbations applied at $\rho_{norm} >= 0.7$. To use electro-magnetic perturbations in the whole domain, one may need to have a closer look at the output from TGLF and use new recommended settings in [3] to filter spurious modes. In the plot below, n_imp_spec1 is the He density, n_imp_spec2 is the Ne density and n_imp_spec3 is the W density.

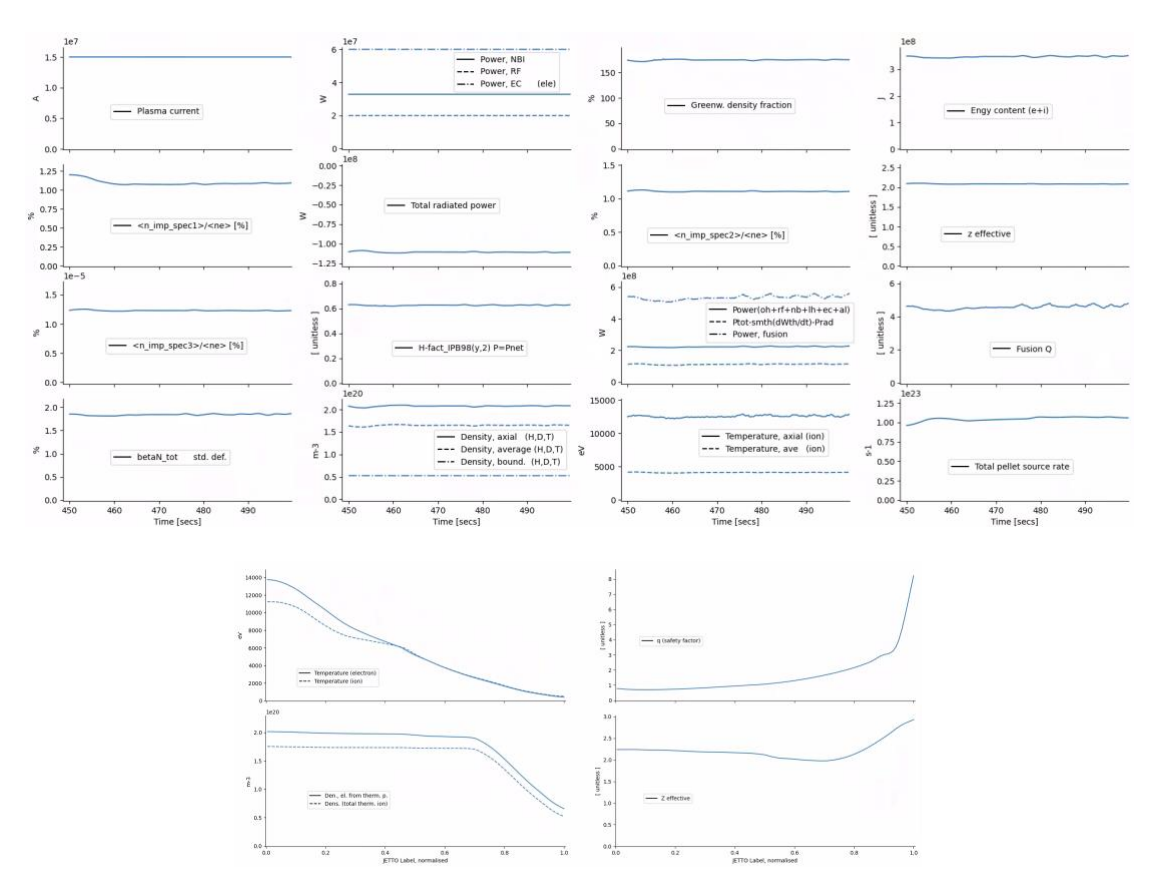
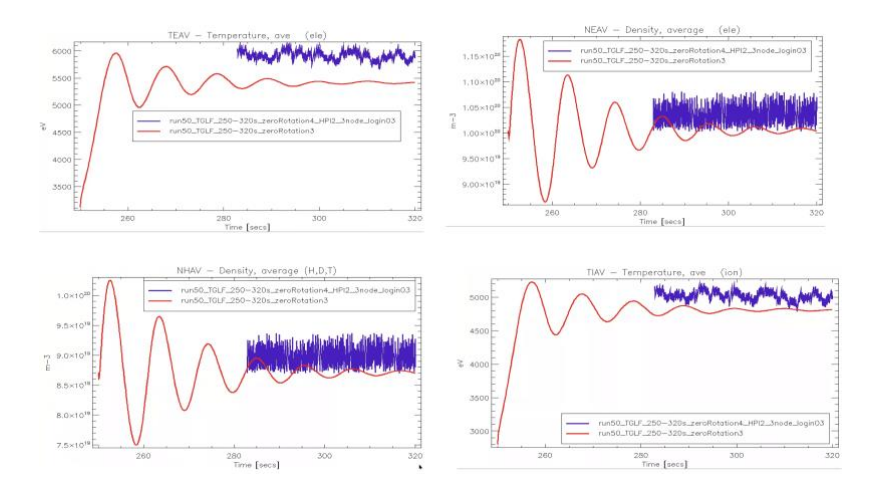


FIG. 3. Time traces of parameters of interest predicted by JETTO with the TGLF-SAT2 model and the SANCO model for the simulation case run54 listed in Table 3 with $Z_{eff} = 2.2$, with $P_{aux} = 113$ MW, $f_{GW} = 175\%$ and $P_{rad}/P_{inp} = 0.1$. Profiles of the electron temperature, ion temperature, safety factor, total thermal ion density and Z_{eff} at the end of the simulation are also shown.

3.4 Results with continuous v.s. discrete pellet model

In this section, the continuous pellet particle deposition model is replaced with the HPI2 pellet model to predict pellet ablation and deposition self-consistently, with TGLF-SAT2 transport model predicting transport process self-consistently both before and after pellet injection. The simplified interpretive model is adopted for impurity transport.

Comparisons of results obtained with the continuous pellet model and HPI2 module are shown in figure 4-5. The averaged electron density can reach the target value with both pellet models through feedback control as shown in figure 4. The averaged ion densities also reach a quasi-steady state value and oscillate with a similar amplitude with electron density as expected. The averaged electron and ion temperatures in the case with the discrete pellet model are higher than those with the continuous pellet model, because in the former case the predicted energy confinement is better. However, Q_{fus} decreases slightly when changing to the discrete pellet model, because the main ion densities on magnetic axis are lower than that with the continuous pellet model, although the ion temperature on axis is slightly higher. The lower main ion density and higher ion temperature on axis with the discrete pellet model may be explained by the larger positive density gradient caused by the pellet deposition, which suppresses turbulence and reduces the inward particle transport. This was investigated for the ITER baseline H-mode plasma [4]. In comparison, the resulting positive density gradient is smaller with a time-averaged pellet source in the continuous pellet model. These can be seen in figure 5. Due to the same reason, the density peak at the edge in the discrete pellet model will build up instead of disappearing with time as in the continuous pellet model. The improved calculations with higher time resolution are being carried out which may show a reduced edge peak as increased particle transport just after pellet injection when the gradients are very high are better resolved in the new runs. It is predicted that the outward energy transport will also reduce in the same region with the discrete pellet model, forming a relatively strong temperature gradient in this region, which is like an inward shifted pedestal.



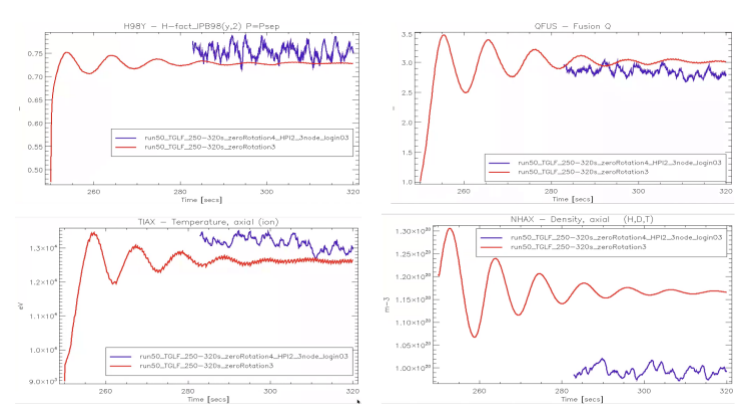


FIG. 4. Time traces of the averaged T_e , n_e , n_i , T_i , the energy confinement factor H98(y, 2), the fusion gain Q_{fus} , the axial T_i and n_i predicted by JETTO with the continuous pellet model (red) and HPI2 module (blue) respectively based on the simulation case run50 listed in Table 2. In this case, $P_{aux} = 60 \text{ MW}$, $f_{GW} = 90\%$ and $P_{rad}/P_{inp} = 0.3$. TGLF-SAT2 is adopted to predict transport process of main particles self-consistently. The simple interpretive model is used for impurity transport.

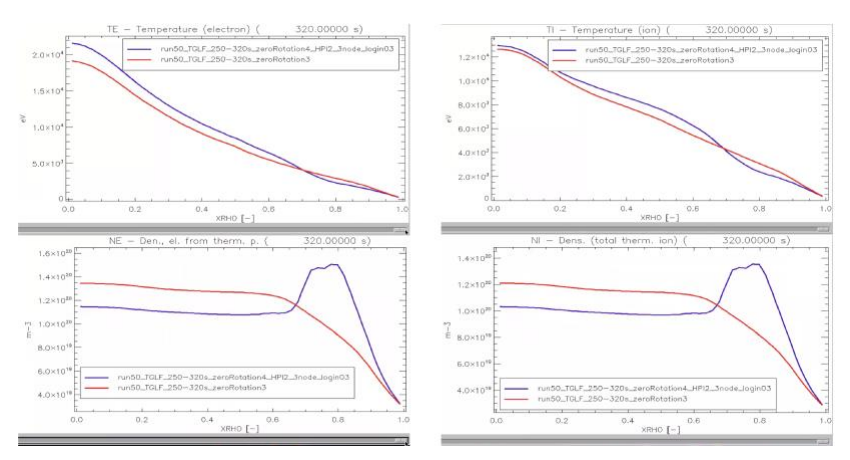


FIG 5. Profiles of electron temperature T_e , ion temperature T_i , electron density n_e , and total thermal ion density n_i predicted by JETTO at the end of the simulation with the continuous pellet model (red) and HPI2 module (blue) respectively based on the simulation case run50 listed in Table 2.

The main reasons for optimistic predictions of fusion performances such as P_{fus} and Q_{fus} in high density L-mode are as follows. (1) Strong increase of P_{fus} with density ($P_{fus} \propto n^2$). (2) Confinement is predicted to be above the L-mode scaling, which is typically $H <= \sim 0.5$. Even though the plasma is in L-mode, there is some kind of an edge pedestal present after pellet injection at least in terms of the density, which features a large edge gradient due to enhanced pellet fueling. (3) High charge exchange heat flux at high density provides high T_i in core although with very high fraction of heat input applied to electrons in EC heating regime. T_i clamping reported for EC heated ITER and DEMO cases with TGLF-SAT2 [5] might not be applicable for high density L-mode. (4) Deeper pellet penetration is expected in L-mode plasma compared to reactor H-mode due to smaller edge temperatures, which may lead to better particle confinement due to deep particle deposition, although plasmoid drift in L-mode plasma is expected to be reduced.

4. CONCLUSIONS

In this work, we adopt JINTRAC integrated modeling suite to investigate the possibility of high Q L-mode plasma operation for ITER, by optimizing some actuators, including auxiliary heating power, radiation fraction and Greenwald density fraction which is feedback controlled by pellet injection. Overall, high auxiliary heating power, high density and low radiation fraction is beneficial to fusion performances.

In addition, simulation results obtained with the Bohm-gyro-Bohm scaling-based model are compared against the TGLF-SAT2 model, the interpretive impurity model against the predictive SANCO impurity transport model, and the continuous pellet model against the discrete pellet model based on the HPI2 code. The confinement in ITER high density L-mode predicted by the TGLF-SAT2 model is much better than that with the BgB scaling-based model, resulting in a significantly larger Q. Fusion performances such as P_{fus} and Q change only slightly when changing from the interpretive impurity model to the predictive SANCO model, or changing from the continuous pellet model to the discrete HPI2 pellet model, although the plasma density and temperature profiles can have a significant difference. This relaxes the concern that simulation studies in literatures based on the continuous pellet model may lead to problematic conclusions in terms of fusion performances for ITER. The highest Q obtained for these ITER high density L-mode simulations is \sim 5, which is quite amazing and reveals the potentials of high Q L-mode operation for ITER and future demo reactors.

Regarding a possible solution for the divertor that would be compatible with the high density high power L-mode plasmas shown in this work, there are some stationary core solutions that have been run with JETTO-SANCO that would fit with the XPR solution in [6] and that are not far away from the conditions of our L-mode plasma simulations, so an integrated core-edge-SOL solution for the L-mode cases shown in this work should be viable.

ACKNOWLEDGMENTS

This work was supported by MCF Energy R&D Program of China under Contract Nos. 2024YFE03270200, 2022YFE03090003, the National Natural Science Foundation of China under Contract Nos. 12475227, 12205196, "USTC Research Funds of the Double First-Class Initiative" under Contract No. YD2140002005. Disclaimer: ITER is the Nuclear Facility INB no. 174. The views and opinions expressed herein do not necessarily reflect those of the ITER Organization.

REFERENCES

- [1] Cenacchi G and Taroni A 1988 JETTO: A free-boundary plasma transport code (basic version) report JET-IR (88) 03 JET joint undertaking *Joint European Torus*
- [2] Pacher H, Kukushkin A, Pacher G, Kotov V, Pitts R and Reiter D 2015 Impurity seeding in ITER DT plasmas in a carbon-free environment *Journal of nuclear materials* **463** 591-5
- [3] Najlaoui A, Camenen Y, Bourdelle C and Loarte A 2025 Verifying turbulence model reduction in high β tokamak plasmas *Plasma Physics and Controlled Fusion* **67** 045016

IAEA-TH-P/3025

- [4] Orrico C A, van Berkel M, Bosman T, Ceelen L, Heemels W, Koechl F and Krishnamoorthy D 2025 Predictive density profile control with discrete pellets, applied to integrated simulations of ITER *Nuclear Fusion*
- [5] López G S, Tardini G, Fable E, Siccinio M and Zohm H 2024 The feasibility of the LH transition for a purely electron-heated EU-DEMO tokamak *Nuclear Fusion* **64** 126012
- [6] Takenaga H and Team J- 2001 Improved particle control for high integrated plasma performance in Japan Atomic Energy Research Institute Tokamak-60 Upgrade *Physics of Plasmas* **8** 2217-23